Author Manuscript

Author Manuscript

Author Manuscript

Author Manuscript

HHS Public Access

Author manuscript

*Cell Rep*. Author manuscript; available in PMC 2019 June 20.

Published in final edited form as:

*Cell Rep*. 2014 November 20; 9(4): 1528–1537. doi:10.1016/j.celrep.2014.10.040.

# Systematic perturbation of cytoskeletal function reveals a linear scaling relationship between cell geometry and fitness

**Russell D. Monds**[1,2,*,‡], **Timothy K. Lee**[2], **Alexandre Colavin**[2], **Tristan Ursell**[2], **Selwyn Quan**[1], **Tim F. Cooper**[3], and **Kerwyn Casey Huang**[1,2,4,*]

[1]Bio-X Program, Stanford University, Stanford, CA 94305, USA

[2]Department of Bioengineering, Stanford University, Stanford, CA 94305, USA

[3]Department of Biology and Biochemistry, University of Houston, Houston, TX 77204, USA

[4]Department of Microbiology and Immunology, Stanford University School of Medicine, Stanford, CA 94305, USA

## Abstract

Diversification of cell size is hypothesized to have occurred through a process of evolutionary optimization, but direct demonstrations of causal relationships between cell geometry and fitness are lacking. Here, we identify a mutation from a laboratory-evolved bacterium that dramatically increases cell size through cytoskeletal perturbation and confers a large fitness advantage. We engineer a library of cytoskeletal mutants with different sizes, and show that fitness scales linearly with respect to cell size over a wide physiological range. Quantifying the growth rates of single cells during exit from stationary phase revealed that transitions between 'feast-famine' growth regimes are a key determinant of cell size-dependent fitness effects. We also uncovered environments that suppress the fitness advantage of larger cells, indicating that cell size-dependent fitness effects are subject to both biophysical and metabolic constraints. Together, our results highlight laboratory-based evolution as a powerful framework for studying the quantitative relationships between morphology and fitness.

## Introduction

Enormous diversity in cell shape and size exists across all kingdoms of life (Calder, 1984; Thompson, 1961). However, for any one species, mechanisms have evolved to robustly regulate and maintain the dimensions of cells or cell types within narrow limits, suggesting that cell geometry is under strong stabilizing selection (Lecuit and Le Goff, 2007; Loehlin and Werren, 2012; Peters, 1986; Young, 2006). Previous studies have reported correlations between fitness and specific cell geometries, but have provided relatively little insight into the mechanistic basis of this relationship (Jiang et al., 2005; Lenski and Travisano, 1994; Lin et al., 2013; Trotta et al., 2007). Cellular dimensions can impact a diverse array of phenotypes via the spatial distribution and concentration of proteins (Llopis et al., 2010; Mondal et al., 2011), regulation of gene expression (Mileyko et al., 2008; Scott et al., 2010;

*Corresponding authors: Russell D. Monds, rmonds@syntheticgenomics.com, Kerwyn Casey Huang, kchuang@stanford.edu.
‡Current address: Synthetic Genomics Inc., 11149 North Torrey Pines Rd, La Jolla, CA 92037, USA.

Author Manuscript Author Manuscript Author Manuscript Author Manuscript

Wu et al., 2010), and physical interactions between the cell and its environment (Cho et al., 2007). Such global phenotypic consequences reinforce the intuitive connection between cell geometry and fitness, but also underscore the challenge in understanding the relationship between these two complex traits. For example, it has proven difficult to systematically manipulate cell geometry while minimizing confounding effects on other traits. As a result, studies have generally been limited to examination of existing populations and indirect correlations between cell geometry and other measurable traits (Young, 2006). The development of approaches for determining the causal relationships between cell geometry and fitness would offer the potential to reveal important physical and biological constraints on the evolution of morphogenesis.

Experimental evolution offers a powerful platform to test evolutionary theories and to examine the causal relationships between mutations, traits, and selection (Blount et al., 2012; Elena and Lenski, 2003; Meyer et al., 2012). A remarkable finding from a long-term evolution experiment was that the bacterium *Escherichia coli* evolved to become much larger in size after 10,000 generations of evolution (Lenski and Travisano, 1994; Lenski et al., 1998; Travisano et al., 1995a); cells from each of twelve independent populations approximately doubled in volume relative to their common ancestor. Intriguingly, changes in cell size were strongly correlated with step-like increases in mean population fitness (Elena et al., 1996). Subsequent studies demonstrated that many of the evolved populations harbored a mutation in *mrdA*, a gene involved in cell-wall synthesis. Two different *mrdA* alleles were shown to be adaptive, conferring a significant fitness advantage relative to the ancestor and explaining a substantial fraction of the increased cell size of evolved clones (Philippe et al., 2009). Although these studies highlight experimental evolution as an invaluable approach for studying the selective value of cell shape, many questions remain unanswered. For example, the underlying basis for selection of increased cell size in experimentally evolved populations is not understood. Furthermore, it remains possible that *mrdA* mutations are pleiotropic and that changes in cell shape are an indirect consequence of selection for another trait.

Regulation of bacterial growth is complex and has been the focus of much research (reviewed in (Sun and Jiang, 2011; Typas et al., 2012)). The cell wall is a macromolecular network that balances the forces on the inner membrane due to turgor pressure and is largely responsible for defining cell shape in most bacteria (Höltje, 1998). The cellular factors that contribute to cell-wall biosynthesis fall into four major classes: 1) Mur enzymes, which synthesize the building blocks of the cell wall (muropeptides) in the cytoplasm; 2) penicillin binding proteins (PBPs), which incorporate muropeptides into the cell-wall network from outside the cytoplasmic membrane; 3) hydrolytic enzymes that cleave bonds in the cell wall (Singh et al., 2012) and 4) cytoskeletal proteins (e.g., MreB, FtsZ), which regulate the spatiotemporal pattern of cell-wall synthesis. MreB is a prokaryotic actin homolog found in many rod-shaped bacteria that forms dynamic structures in the cytoplasm that bind the inner membrane (Dominguez-Escobar et al., 2011; Garner et al., 2011; Salje et al., 2011; van Teeffelen et al., 2011). MreB is thought to coordinate the spatial pattern of insertion of new material into the cell wall during rod-shaped elongation through protein-protein interactions. MreB is essential, and its depletion causes cells to grow as spheres and eventually lyse (Bendezú and de Boer, 2008; Jones et al., 2001).

Author Manuscript Author Manuscript Author Manuscript Author Manuscript

In this study, we use experimentally evolved populations of *E. coli* to examine the relationship between cell geometry and competitive fitness. We identified a single substitution in MreB that confers a large increase in both cell size and fitness relative to the ancestor. Population- and single cell-level growth analyses combined with fine-scale fitness mapping indicated that increased cell size is correlated with faster acceleration of growth upon exit from stationary phase. To systematically define the relationship between cell size and competitive fitness, we developed a genetic approach to tune cell geometry over a wide physiological range. We show that competitive fitness increases linearly as a function of cell size until an upper size limit, whereupon fitness plateaus, or may even decline. Finally, our analysis uncovered environments that suppress the fitness advantage of *mreB* mutants while maintaining their larger cell size, suggesting that the selective advantage of larger cells in experimentally evolved populations is dependent on both metabolic and biophysical parameters.

## Results

### Potential for dramatic changes in cell size during experimental evolution

Previously, we reported the isolation and characterization of 46 clones derived from 24 populations evolved in one of four different carbon-limited environments: glucose (Glu), lactose (Lac), glucose and lactose presented simultaneously (G+L), or glucose and lactose presented on alternate days (G/L) (Quan et al., 2012). To assess whether cell geometry had generally changed through the course of evolution, we performed single-cell imaging of these clones during growth in their evolution environments and extracted distributions for cell width and length (Fig. 1, Table S1). We found that the majority of clones across all four evolution environments showed a mean width increase of 0.05 to 0.15 μm relative to the ancestor (Anc). Our results also suggest that mean cell length increased for the majority of evolved clones, with increases ranging from 0.20 to 1.60 μm. Notably, two clones showed increases in mean width substantially larger than the other evolved clones. Clone G1-2 (evolved in Glu) had a mean width of 0.92 ± 0.05 μm (standard deviation (SD)) and clone G +L3 (evolved in G+L) had a mean width of 0.96 ± 0.05 μm (SD), approximately 0.19 and 0.26 μm greater than the ancestor in Glu and G+L, respectively (Fig. 1, Table S1).

### An *mreB* mutation underlies the increased cell width of an evolved clone

We focused our attention on evolved clone G+L3 since it demonstrated the largest morphological change relative to the ancestor (Fig. 1, red arrow). Quantification of replicate independent cultures of clone G+L3 confirmed a 37% increase in average cell width and no measurable difference in average cell length relative to the ancestor (Fig. 2). Whole-genome sequencing of clone G+L3 revealed seven mutations in the genes or gene regions *rbsDACB, ECB_00822*, *lacO1*, *fabF*, *sapF*, *malT*, and *mreB* (Quan et al., 2012). The *mreB* mutation is a G to A transition at nucleotide position 157 that results in an alanine to threonine substitution at residue 53 ($mreB^{A53T}$). Given the central role of MreB in rod-shaped growth, we reasoned that the $mreB^{A53T}$ allele might explain, at least in part, the increased size of the G+L3 clone. To test this hypothesis, we reconstructed the $mreB^{A53T}$ allele in the ancestral background and compared its morphology to the ancestor and to evolved clone G+L3 (Fig. 2). We found that the $mreB^{A53T}$ allele was necessary and sufficient to account for the

Author Manuscript Author Manuscript Author Manuscript Author Manuscript

increases in cell width of clone G+L3 (average of mean cell width across populations: G +L3, 0.96 ± 0.01 μm (standard error of the mean (SEM)); *mreB*$^{A53T}$, 0.95 ± 0.01 μm (SEM); one-tailed *t*-test, $t_{(4)} = 1.3$, $p = 0.14$). Reversion of the *mreB*$^{A53T}$ allele in clone G+L3 to the ancestral allele resulted in a mean cell width similar to that of the ancestor (average mean cell width: Anc, 0.72 ± 0.01 μm (SEM); G+L3 *mreB*$^{anc}$, 0.74 ± 0.01 μm (SEM)).

Interestingly, the *mreB*$^{A53T}$ allele also conferred a significant reduction in cell length (average mean cell length: Anc, 3.06 ± 0.04 μm (SEM); *mreB*$^{A53T}$, 2.50 ± 0.02 μm (SEM); one-tailed *t*-test, $t_{(4)} = 13.6$, $p < 0.001$), suggesting that other mutations in the G+L3 background act to increase mean cell length. In support of this hypothesis, reversion of the *mreB*$^{A53T}$ allele in clone G+L3 conferred a mean cell length substantially greater than the ancestor (Fig. 2B). Nevertheless, the large width increase conferred by the *mreB*$^{A53T}$ allele resulted in a substantial increase in cell volume (37%) and surface area (10%) relative to the ancestor despite the small decrease in cell length (Fig. 2C). Reductions in the ratio of cellular surface area to volume (SA/V) resulting from increases in cell width are often cited as a fundamental constraint on cell size. Consistent with its larger cell size, the *mreB*$^{A53T}$ strain has reduced SA/V relative to the ancestor (Ancestor, 4.36 ± 0.28 $\mu m^{-1}$) (SEM); *mreB*$^{A53T}$, 6.00 ± 0.25 $\mu m^{-1}$ (SEM)).

## The *mreB*$^{A53T}$ allele is adaptive

To determine the fitness effect of the *mreB*$^{A53T}$ mutant, we competed it against the ancestor in all four environments used in the evolution experiment (Fig. 3, Methods). We found that the *mreB*$^{A53T}$ allele conferred a large fitness benefit in all environments that included glucose (Glu, G+L, and G/L) and a small but significant fitness benefit in Lac (relative fitness and two-tailed *t*-test: Glu, 10.2%, $t_{(7)} = 51.7$, $p < 0.001$; Lac, 0.9%, $t_{(7)} = 11.9$, $p < 0.001$; G+L, 6.1%, $t_{(7)} = 16.7$, $p < 0.001$; G/L, 11%, %, $t_{(7)} = 24.7$, $p < 0.001$). To rule out the possibility that these fitness effects were due to secondary mutations that could have been acquired during strain construction, we confirmed that similar results were obtained with an independently constructed *mreB*$^{A53T}$ strain, and that reversion of the *mreB*$^{A53T}$ allele back to the ancestral sequence resulted in a strain with competitive fitness equivalent to that of the ancestor (Fig. S1).

## The *mreB*$^{A53T}$ allele confers a lag-phase growth advantage

In the evolution experiment, populations transited through four distinct phases of growth during each daily transfer cycle: 1) lag phase, a period of physiological acclimation to a nutrient upshift; 2) exponential phase, a period of sustained growth at a constant rate; 3) transition phase, when depletion of the limiting resource begins to restrict growth; and 4) stationary phase, when the concentration of the limiting resource cannot support further growth (Vasi et al., 1994). As a foundation from which to probe the physiological changes conferred by the *mreB*$^{A53T}$ allele, we first sought to understand its effect on each of these phases. To do this, we quantified the growth dynamics of the ancestral and *mreB*$^{A53T}$ strains at population and single-cell levels when grown in Glu, the single resource environment in which the *mreB*$^{A53T}$ allele showed the largest fitness effect (Fig. 4). Population-level growth analysis demonstrated that maximal exponential growth rates did not significantly differ (Anc $\mu_{max} = 0.519 \pm 0.015$ $hr^{-1}$ (SEM); *mreB*$^{A53T}$ $\mu_{max} = 0.516 \pm 0.007$ $hr^{-1}$ (SEM); two-

Author Manuscript Author Manuscript Author Manuscript Author Manuscript

tailed *t*-test, $t_{(10)} = 0.19$, $p = 0.86$). However, the duration of the lag phase of the *mreB*$^{A53T}$ strain was ~0.8 hr shorter than that of the ancestor (Fig. 4A), and this difference was highly significant (Anc lag = 2.28 ± 0.11 hr (SEM); *mreB*$^{A53T}$ lag = 1.47 ± 0.08 hr (SEM), two-tailed *t*-test, $t_{(10)} = 6.4$, $p < 0.001$). A similar trend was observed when viable cell counts were used to estimate the length of lag phase for the ancestral and *mreB*$^{A53T}$ strains (Anc lag = 2.01 hr (SEM); *mreB*$^{A53T}$ lag =1.60 hr (SEM); Fig. S2). To complement these bulk measurements, we used time-lapse imaging to quantify single-cell growth rates for the ancestral and *mreB*$^{A53T}$ strains during the transition from stationary phase to exponential growth on DM+Glu media (Fig. 4B,C). Although the two strains initiated growth at similar times, the growth rate of the *mreB*$^{A53T}$ strain accelerated faster than that of the ancestor, thereby reaching its maximum growth rate sooner (Anc, $t_{V½max}$ = 76 ± 6 min (SEM); *mreB*$^{A53T}$, $t_{V½max}$ = 36 ± 4 min (SEM).

Taken together, our growth analyses suggest that the *mreB*$^{A53T}$ allele confers a fitness advantage during the transition from stationary phase to exponential growth. We tested this prediction by quantifying the differential growth of the *mreB*$^{A53T}$ strain relative to the ancestor over the course of a single competitive cycle by designing a protocol that measures the temporal trajectory of fitness effects (Methods). As a negative control for this assay, the ancestor showed no differential growth throughout the course of competition when competed against itself (Fig. 4D). By contrast, the *mreB*$^{A53T}$ strain exhibited positive differential growth after as little as 2 hr of competition against the ancestor (competitive differential growth at 2 hr, two-tailed *t*-test: Anc, 0.02 ± 0.06 (SEM), $t_{(7)} = 0.32$, $p = 0.766$; *mreB*$^{A53T}$, 0.24 ± 0.05 (SEM), $t_{(7)} = 5.9$, $p = 0.002$). After 6 hr of competition, the differential growth of the *mreB*$^{A53T}$ strain reached values similar to the total gains measured over a complete 24-hr cycle (Fig. 4D). These competition data reinforce the hypothesis generated by our growth data that a significant component of the fitness advantage conferred by the *mreB*$^{A53T}$ allele occurs during lag phase, specifically by accelerating the transition to exponential growth.

## Fitness scales linearly with cell geometry

When competed in glucose containing environments, the *mreB*$^{A53T}$ allele confers a sizeable fitness advantage over the ancestor. However, as with previous studies correlating cell morphology and fitness, it is not clear whether the morphological effect of the *mreB*$^{A53T}$ allele is the trait under direct selection or whether the *mreB*$^{A53T}$ allele is pleiotropic, with selection acting on a trait other than cell size. To address this fundamental evolutionary question, we sought to examine how fitness scales as a function of cell geometry. We reasoned that different amino acids at the 53$^{rd}$ residue of MreB might confer a range of stable changes in cell width that would allow us to examine the correlation between fitness and cell geometry. To explore this possibility, we screened various A53 alleles using *trans* complementation of an *mreB* null mutant (Methods). Many of the 19 possible *mreB*$^{A53}$ substitutions conferred changes in cell shape and size. We selected eight *mreB*$^{A53}$ alleles that conferred a broad range of stable and uniform changes to cell width, and engineered them into the chromosome of our ancestral strain, REL606. Single-cell analysis confirmed that our collection of REL606 *mreB*$^{A53}$ strains conferred cell widths distributed relatively uniformly from 0.71 μm to 1.10 μm (Fig. 5A).

Author Manuscript Author Manuscript Author Manuscript Author Manuscript

Next, we assessed the fitness of each *mreB* mutant strain relative to the ancestor when grown in the Glu environment. Fitness increased approximately linearly with increasing cell width up to ~0.94 μm, the width of the *mreB*$^{A53T}$ strain, after which further increases in cell width did not cause any further increase in relative fitness (Fig. 5B, S4). Consistent with the observations presented in Fig. 2, there was a negative correlation between the width and length of the *mreB*$^{A53}$ strains (Pearson correlation: r = −0.90, $p < 0.001$, Fig. S3). Nonetheless, the fractional width increase was more substantial than the fractional length decrease, and thus cell volume scaled with fitness in a similar manner to cell width (Fig. S3). We note that other cell attributes (volume, surface area and surface area-to-volume ratio) show a similar relationship to fitness as does cell width (Fig. S3). Overall, the robust scaling between fitness and cell geometry is consistent with selection acting directly on changes in geometry that result from perturbations of MreB cytoskeletal function.

## Physiological limits to cell size-dependent fitness benefits

The breakdown in the positive correlation between fitness and geometry at large cell sizes could be due to tradeoffs that offset further fitness gains from increased cell size, or to physiological saturation of the biological mechanism responsible for cell size-dependent fitness increases. To assess the relative contributions of these effects, we measured the population-level growth dynamics of the *mreB*$^{A53}$ strains in DM+Glu and compared the maximal growth rates and lag times as a function of mean cell width. We observed no significant correlation between cell width and maximal growth rate (Pearson correlation: $r = -0.28$, $p = 0.44$, Fig. 5C). In contrast, lag time was inversely correlated with cell width (Pearson correlation: $r = -0.83$, $p = 0.003$, Fig. 5D). Similar to the relationship between cell width and fitness (Fig. 5B), decreases in lag time began to level off as cell width approached ~0.9 μm (Fig. 5D). This observation is more consistent with physiological saturation of cell size-dependent fitness effects as cells tend toward an upper bound. However, we cannot formally rule out the possibility that pleiotropic effects act to counter further cell size-dependent decreases in lag phase.

## Environmental dependence of cell-size fitness effects

During competition against the ancestor in the Lac environment, the *mreB*$^{A53T}$ allele was nearly neutral (Fig. 3), in contrast to the large fitness effects seen in the three glucose-containing environments (Glu, G/L, and G+L). Differences in fitness effects did not reflect an environmental dependence of the morphological effect of the *mreB*$^{A53T}$ allele; when grown in Lac, both exponentially growing cells and stationary phase cells of the *mreB*$^{A53T}$ strain exhibited values for mean cell width and length similar to values resulting from growth in Glu (Fig. S4). Our data suggest that faster acceleration into exponential growth is a necessary component of the fitness advantage conferred by the *mreB*$^{A53T}$ allele in the Glu environment. Consistent with this hypothesis and the environmental dependence of fitness gains, single-cell growth analysis in the Lac environment demonstrated that the *mreB*$^{A53T}$ strain does not exhibit a lag phase growth advantage relative to the ancestor (Anc, $t_{V½max}$ = 160 ± 10 min; *mreB*$^{A53T}$, $t_{V½max}$ = 160 ± 12 min; Fig. S4).

To determine whether the benefit of the *mreB*$^{A53T}$ allele is specific to glucose-containing environments, we measured the fitness of the *mreB*$^{A53T}$ strain relative to the ancestor in

Author Manuscript Author Manuscript Author Manuscript Author Manuscript

eight additional environments (fructose, N-acetylglucosamine, mannitol, mannose, trehalose, galactose, melibiose, and maltose). These carbon sources were chosen based on a previous experimental evolution study that revealed a pattern of fitness effects that correlated with the mechanism of substrate uptake (Travisano and Lenski, 1996). We determined the morphological effect of the *mreB*$^{A53T}$ allele in each environment and in all cases found that it conferred a ~30% increase in cell width, in addition to a ~25% decrease in cell length (Fig. 6A). Interestingly, the *mreB*$^{A53T}$ mutant demonstrated a fitness advantage relative to the ancestor in all environments containing sugars transported by the phosphotransferase system (PTS), with a benefit similar to that realized in Glu for all environments except mannose (Fig. 6B). In contrast, when competed in environments with non-PTS sugars like Lac, we observed a wide range of fitness effects for the *mreB*$^{A53T}$ mutant; a fitness cost in galactose, a small benefit in maltose, and an advantage in melibiose of similar magnitude to that seen in Glu. We did not observe a correlation between fitness and the mechanism of transport through the outer membrane (OmpF vs. LamB). For example, the fitness advantage conferred by the *mreB*$^{A53T}$ allele when competed in the trehalose environment (PTS/LamB) was comparable to fitness effects in the majority of PTS/OmpF environments. Irrespective of the role of transport, the morphological effect of the *mreB*$^{A53T}$ allele appears to be general to all growth conditions, whereas fitness of the *mreB*$^{A53T}$ allele varies considerably across a broad range of carbon sources.

## Discussion

Here, we used experimentally evolved populations of bacteria to probe the relationship between cell geometry and fitness. Strikingly, a single amino acid substitution in MreB, a prokaryotic actin homolog, conferred large increases in both cell width and fitness relative to the ancestor. Based on this finding, we devised a strategy to systematically tune the geometry of *E. coli* cells, and provided the first demonstration that competitive fitness in a laboratory environment increases monotonically as a function of cell width over a wide range. The ability to tune cell geometry through minimal genetic manipulation offers the potential to quantitatively explore the effects of various morphological states in a manner that is well controlled and limits the influence of indirect effects.

It is usually difficult to interpret the evolutionary relevance of genotype-phenotype relationships; in this respect, experimental evolution provides the opportunity to examine the causative connections between genotype-phenotype relationships and natural selection. Here, we demonstrate that differences in lag-phase growth dynamics are a key determinant of the fitness advantage conferred by various *mreB*$^{A53}$ alleles. The exact processes that govern lag phase will depend on the nature of the environmental shift, but in the aggregate, these processes determine the rate with which a cell tends toward its maximal growth rate. Classical analyses of lag phase have tended not to distinguish between differences in the period of latency and in the rate of acceleration toward $\mu_{max}$, largely due to the lack of temporal resolution or sensitivity of the methodologies employed. To investigate this distinction, we used time-lapse microscopy to quantify the dynamics of single-cell growth rates and demonstrated that during regrowth in fresh media, the ancestral and *mreB*$^{A53T}$ strains initiate growth at similar times, but the *mreB*$^{A53T}$ strain accelerates more quickly to its maximal growth rate.

Author Manuscript Author Manuscript Author Manuscript Author Manuscript

For most bacteria in nature, lag-phase growth dynamics and the ability to respond to changes in the availability of nutrients are likely of immense importance for competitive fitness in complex, dynamic environments (Kussell and Leibler, 2005). However, the mechanistic determinants of lag phase are generally not well understood (Rolfe et al., 2012). What properties of larger cells facilitate the lag-phase advantage we have observed? Lenski and colleagues have suggested that increased surface area may facilitate nutrient uptake at rates faster than the nutrient can be catabolized, thereby resulting in energy reserves that confer a benefit in the feast-famine regime of the evolution environment (Lenski et al., 1998; Philippe et al., 2009). Indirect support for this hypothesis comes from studies of experimentally evolved populations in which reduction in lag phase was an important component of increases in mean population fitness (Vasi et al., 1994) and that glucose transport was inferred as a possible target of selection (Travisano and Lenski, 1996; Travisano et al., 1995b). This model is supported by the geometric scaling of cell size and fitness we have demonstrated, and is consistent with our observed upper bound for reductions in lag time as a function of increased cell size, perhaps because other aspects of glucose catabolism becoming limiting when the effective transport rate passes a certain threshold. Nonetheless, the carbon-source dependence of the fitness advantage conferred by the *mreB*$^{A53T}$ allele indicates that fitness benefits do not always scale simply with cellular surface area and the associated increases in transporter copy number. An alternative hypothesis is that larger cells accommodate higher amounts of DNA; during lag phase, extra genomic content could jump-start cell growth and division. However, we observed that the fractions of stationary-phase cells with one or two copies of DNA were similar for the ancestor and *mreB*$^{A53T}$ mutant (Fig. S5), suggesting that the amount of DNA may not be the underlying cause of the size-dependent fitness effects we have observed. Turgor pressure may also stretch the wall more in cells with larger widths, providing a mechanical stimulus for the acceleration from lag phase to exponential growth, motivating future examination of cell-wall composition (Desmarais et al., 2013) and elongation dynamics of cells grown in different carbon sources. Our suite of variably sized *mreB*$^{A53}$ strains will provide a valuable resource for hypothesis testing since the physiological effects underlying their fitness advantage should scale with cell size over a well-defined geometric range. The ability to modulate cell size through mutation of a single locus in an otherwise isogenic background minimizes the likelihood of confounding effects due to differential pleiotropy and epistasis.

A notable finding from this study is that fitness effects of changes in cell size of *E. coli* vary over a large range depending on the carbon source in the environment. Importantly, differences in fitness effects were not due to differences in the effect of the *mreB*$^{A53T}$ allele on cell size. Of the carbon sources we tested, PTS substrates tended to supported higher cell-size fitness effects relative to non-PTS substrates. We do not currently know what aspects of PTS/non-PTS substrate transport and subsequent metabolism could explain these observations, but it is clear that the mechanisms underlying cell size-fitness effects are subject to both metabolic and biophysical constraints. For example, if increases in surface area generally facilitate increased nutrient uptake, the impact on fitness must somehow be weighted by the specifics of substrate transport and/or metabolism.

The MreB cytoskeleton plays a central role in directing cell-wall synthesis (Wang et al., 2012) and architecture (van Teeffelen et al., 2011), and also contributes to cellular stiffness

Author Manuscript Author Manuscript Author Manuscript Author Manuscript

(Wang et al., 2010) and membrane organization (Strahl et al., 2014). Despite recent advances, it remains unclear what molecular interactions are important for MreB-dependent regulation of cell geometry or how these interactions are integrated with other morphogenetic processes. In this regard, it has not escaped our notice that enrichment of cell-shape mutations during experimental evolution offers a unique genetic resource to probe the mechanistic basis of morphogenesis. In this study, examination of laboratory-evolved populations resulted in the identification of substitutions at a single residue of MreB that can tune the width of *E. coli* over a wide range. Understanding the mechanistic basis of this effect offers the potential to gain important insight into MreB function and morphogenesis. Molecular dynamics simulations suggest that MreB filaments adopt a nucleotide-dependent curvature (Colavin et al., 2014). One possibility is that substitutions at the 53$^{rd}$ position of MreB change the degree of filament curvature in a graded fashion. Differences in the preferred curvature of MreB filaments coupled to interactions of the filaments with the inner membrane could affect the localization of MreB (Ursell et al., 2014) and the balance of forces during construction of the cell wall, a combination of which ultimately results in changes in cell width. Future studies leveraging cell shape mutations isolated from experimental evolution studies have the potential to shed light on MreB structure, dynamics, and the associated changes in cell-wall composition, and localization of synthesis enzymes.

The large and stable morphological effect of mutations like *mreB*$^{A53T}$ suggests there may be a considerable dynamic range in *E. coli* morphogenesis. Nonetheless, MreB sequence is well conserved (>99% identity) across a diverse range of natural *E. coli* isolates (Broad Institute's *Escherichia coli* Antibiotic Resistance Database), consistent with the hypothesis that selection has optimized cell size. How is a complex network of proteins optimized for building a cell with a specified geometry (specialization), while retaining the ability to explore new, stable morphological regimes (adaptability) (Jiang et al., 2015)? One possibility is that cell morphology is also optimized for functional robustness during growth and division. The synthesis machinery that builds the cell, as well as structural features responsible for maintaining cell shape, must exhibit functional tolerance against genetic and environmental perturbations. Detailed examination of the molecular mechanisms underlying the changes in cell geometry and fitness in experimentally evolved populations should offer insight into how the cell balances the need for precise control over cell geometry with the requirement for robustness during growth and division. We anticipate that future investigations will further probe our surprising observation that despite apparently strong stabilizing selection in nature, large increases in cell size occur and appear to be adaptive in experimentally evolved populations.

## Experimental Procedures

Strains and plasmids used in this study are described in Table S2. For routine culturing, cells were grown in lysogeny broth (LB) medium (Bertani, 2004). Davis minimal (DM) medium was used for experimental evolution and subsequent analysis of evolved clones (Lenski et al., 1991). Sugars were added to base DM medium at the following concentrations to make single and mixed resource environments: Glu, 175 μg/mL; Lac, 210 μg/mL; and G+L, 87.5 μg/mL Glu and 105 μg/mL Lac (Cooper and Lenski, 2010). Strains were grown at 37 ˚C unless stated otherwise. Antibiotics were used at the following concentrations:

Author Manuscript Author Manuscript Author Manuscript Author Manuscript

chloramphenicol (Sigma Aldrich, St. Louis, MO), 15 μg/mL; streptomycin (Sigma Aldrich), 100 μg/mL.

Various *mreB* alleles were introduced onto the chromosome using a suicide plasmid-mediated approach (Philippe et al., 2004). The fitness of test strains were measured using a flow cytometry method described by (Zhang et al., 2012).

Phase-contrast images were acquired for large populations of cells. Custom MATLAB (MathWorks, Natick, MA) image processing code was used to segment cells and to identify cell outlines from phase-contrast microscopy images (Ursell et al., 2014). Measurements of average cell width across a population were highly reproducible, and were validated relative to outlines extracted from cells stained with the membrane dye FM4-64 (Fig. S6). Estimates of error were rounded up to the nearest 10 nm to reflect the precision of our measurements. Single cell growth analysis was performed as described by (Lee et al., 2014). Growth rates for each cell were determined as the fractional change in cell outline area between consecutive frames.

Descriptions of other methods can be found in the Supplemental Information.

## Supplementary Material

Refer to Web version on PubMed Central for supplementary material.

## Acknowledgments

We thank members of the Huang lab for helpful discussions and Trang Duong for technical assistance with fitness assays. This research was supported by a Bio-X Senior Fellowship (to R.D.M.), a Siebel Scholars Graduate Fellowship (to T.K.L.), an NIH Biotechnology Training Grant (to T.K.L.), a Stanford Graduate Fellowship (to A.C.), a Bio-X Postdoctoral Fellowship (to T.S.U.), NSF grant DEB-1253650 (to T.F.C.), and NSF CAREER Award MCB-1149328 (to K.C.H.).

## References

Bendezú FO, and de Boer PAJ (2008). Conditional lethality, division defects, membrane involution, and endocytosis in mre and mrd shape mutants of Escherichia coli. J. Bacteriol. 190, 1792–1811. [PubMed: 17993535]

Bertani G (2004). Lysogeny at mid-twentieth century: P1, P2, and other experimental systems. J. Bacteriol. 186, 595–600. [PubMed: 14729683]

Blount ZD, Barrick JE, Davidson CJ, and Lenski RE (2012). Genomic analysis of a key innovation in an experimental Escherichia coli population. Nature 489, 513–518. [PubMed: 22992527]

Calder WA III (1984). Size, Function, and Life History (Cambridge, MA: Harvard University Press).

Cho H, Jönsson H, Campbell K, Melke P, Williams JW, Jedynak B, Stevens AM, Groisman A, and Levchenko A (2007). Self-Organization in High-Density Bacterial Colonies: Efficient Crowd Control. PLoS Biology 5, e302. [PubMed: 18044986]

Colavin A, Hsin J, and Huang KC (2014). Effects of polymerization and nucleotide identity on the conformational dynamics of the bacterial actin homolog MreB. Proc. Natl. Acad. Sci. USA 111, 3585–3590. [PubMed: 24550504]

Cooper TF, and Lenski RE (2010). Experimental evolution with *E. coli* in diverse resource environments. I. Fluctuating environments promote divergence of replicate populations. BMC Evol. Biol. 10, 11. [PubMed: 20070898]

Author Manuscript Author Manuscript Author Manuscript Author Manuscript

Desmarais SM, de Pedro MA, Cava F, and Huang KC (2013). Peptidoglycan at its peaks: how chromatographic analyses can reveal bacterial cell wall structure and assembly. Mol. Microbiol. 89, 1–13. [PubMed: 23679048]

Dominguez-Escobar J, Chastanet A, Crevenna AH, Fromion V, Wedlich-Soldner R, and Carballido-Lopez R (2011). Processive Movement of MreB-Associated Cell Wall Biosynthetic Complexes in Bacteria. Science 333, 225–228. [PubMed: 21636744]

Elena SF, Cooper VS, and Lenski RE (1996). Punctuated evolution caused by selection of rare beneficial mutations. Science 272, 1802–1804. [PubMed: 8650581]

Elena SF, and Lenski RE (2003). Evolution experiments with microorganisms: the dynamics and genetic bases of adaptation. Nat Rev Genet 4, 457–469. [PubMed: 12776215]

Garner EC, Bernard R, Wang W, Zhuang X, Rudner DZ, and Mitchison T (2011). Coupled, Circumferential Motions of the Cell Wall Synthesis Machinery and MreB Filaments in B. subtilis. Science 333, 222–225. [PubMed: 21636745]

Höltje JV (1998). Growth of the stress-bearing and shape-maintaining murein sacculus of Escherichia coli. Microbiol. Mol. Biol. Rev. 62, 181–203. [PubMed: 9529891]

Jiang C, Brown PJB, Ducret A, and Brun YV (2015). Sequential evolution of bacterial morphology by co-option of a developmental regulator. Nature 506, 489–493.

Jiang L, Schofield OME, and Falkowski PG (2005). Adaptive evolution of phytoplankton cell size. Am. Nat. 166, 496–505. [PubMed: 16224705]

Jones LJ, Carballido-Lopez R, and Errington J (2001). Control of cell shape in bacteria: helical, actin-like filaments in Bacillus subtilis. Cell 104, 913–922. [PubMed: 11290328]

Kussell E, and Leibler S (2005). Phenotypic diversity, population growth, and information in fluctuating environments. Science 309, 2075–2078. [PubMed: 16123265]

Lecuit T, and Le Goff L (2007). Orchestrating size and shape during morphogenesis. Nature 450, 189–192. [PubMed: 17994084]

Lee TK, Tropini C, Hsin J, Desmarais SM, Ursell TS, Gong E, Gitai Z, Monds RD, and Huang KC (2014). A dynamically assembled cell wall synthesis machinery buffers cell growth. Proc. Natl. Acad. Sci. USA.

Lenski RE, and Travisano M (1994). Dynamics of adaptation and diversification: a 10,000-generation experiment with bacterial populations. Proc. Natl. Acad. Sci. U.S.a. 91, 6808–6814. [PubMed: 8041701]

Lenski RE, Mongold JA, Sniegowski PD, Travisano M, Vasi F, Gerrish PJ, and Schmidt TM (1998). Evolution of competitive fitness in experimental populations of E. coli: what makes one genotype a better competitor than another? Antonie Van Leeuwenhoek 73, 35–47. [PubMed: 9602277]

Lenski R, Rose M, and Simpson S (1991). Long-term experimental evolution in *Escherichia coli*. I. Adaptation and divergence during 2,000 generations. Am. Nat. 138, 1315–1341.

Lin JI, Poon C, and Harvey KF (2013). The Hippo Size Control Pathway--Ever Expanding. Science Signaling 259, pe4.

Llopis PM, Jackson AF, Sliusarenko O, Surovtsev I, Heinritz J, Emonet T, and Jacobs-Wagner C (2010). Spatial organization of the flow of genetic information in bacteria. Nature 466, 77–81. [PubMed: 20562858]

Loehlin DW, and Werren JH (2012). Evolution of Shape by Multiple Regulatory Changes to a Growth Gene. Science 335, 943–947. [PubMed: 22363002]

Meyer JR, Dobias DT, Weitz JS, Barrick JE, Quick RT, and Lenski RE (2012). Repeatability and contingency in the evolution of a key innovation in phage lambda. Science 335, 428–432. [PubMed: 22282803]

Mileyko Y, Joh RI, and Weitz JS (2008). Small-scale copy number variation and large-scale changes in gene expression. Proc. Natl. Acad. Sci. USA 105, 16659–16664. [PubMed: 18946033]

Mondal J, Bratton BP, Li Y, Yethiraj A, and Weisshaar JC (2011). Entropy-based mechanism of ribosome-nucleoid segregation in E. coli cells. Biophys. J. 100, 2605–2613. [PubMed: 21641305]

Peters RH (1986). The Ecological Implications of Body Size (Cambridge: Cambridge University Press).

Author Manuscript Author Manuscript Author Manuscript Author Manuscript

Philippe N, Alcaraz J-P, Coursange E, Geiselmann J, and Schneider D (2004). Improvement of pCVD442, a suicide plasmid for gene allele exchange in bacteria. Plasmid 51, 246–255. [PubMed: 15109831]

Philippe N, Pelosi L, Lenski RE, and Schneider D (2009). Evolution of penicillin-binding protein 2 concentration and cell shape during a long-term experiment with Escherichia coli. J. Bacteriol. 191, 909–921. [PubMed: 19047356]

Quan S, Ray JCJ, Kwota Z, Duong T, Balázsi G, Cooper TF, and Monds RD (2012). Adaptive Evolution of the Lactose Utilization Network in Experimentally Evolved Populations of Escherichia coli. PLoS Genet. 8, e1002444. [PubMed: 22253602]

Rolfe MD, Rice CJ, Lucchini S, Pin C, Thompson A, Cameron ADS, Alston M, Stringer MF, Betts RP, Baranyi J, et al. (2012). Lag Phase Is a Distinct Growth Phase That Prepares Bacteria for Exponential Growth and Involves Transient Metal Accumulation. The Journal of Bacteriology 194, 686–701. [PubMed: 22139505]

Salje J, van den Ent F, de Boer P, and Löwe J (2011). Direct Membrane Binding by Bacterial Actin MreB. Mol. Cell 43, 478–487. [PubMed: 21816350]

Scott M, Gunderson CW, Mateescu EM, Zhang Z, and Hwa T (2010). Interdependence of Cell Growth and Gene Expression: Origins and Consequences. Science 330, 1099–1102. [PubMed: 21097934]

Singh SK, SaiSree L, Amrutha RN, and Reddy M (2012). Three redundant murein endopeptidases catalyse an essential cleavage step in peptidoglycan synthesis of Escherichia coliK12. Mol. Microbiol. 86, 1036–1051. [PubMed: 23062283]

Strahl H, Bürmann F, and Hamoen LW (2014). The actin homologue MreB organizes the bacterial cell membrane. Nature Communications 5, 3442.

Sun SX, and Jiang H (2011). Physics of bacterial morphogenesis. Microbiol. Mol. Biol. Rev. 75, 543–565. [PubMed: 22126993]

Thompson DW (1961). On Growth and Form (Cambridge University Press).

Travisano M, and Lenski RE (1996). Long-term experimental evolution in Escherichia coli. IV. Targets of selection and the specificity of adaptation. Genetics 143, 15–26. [PubMed: 8722758]

Travisano M, Mongold JA, Bennett AF, and Lenski RE (1995a). Experimental tests of the roles of adaptation, chance, and history in evolution. Science 267, 87–90. [PubMed: 7809610]

Travisano M, Vasi F, and Lenski RE (1995b). Long-term experimental evolution in Escherichia coli. III. Variation among replicate populations in correlated responses to novel environments. Evolution 49, 189–200. [PubMed: 28593661]

Trotta V, Calboli FC, Ziosi M, and Cavicchi S (2007). Fitness variation in response to artificial selection for reduced cell area, cell number and wing area in natural populations of Drosophila melanogaster. BMC Evol. Biol. 7, S10.

Typas A, Banzhaf M, Gross CA, and Vollmer W (2012). From the regulation of peptidoglycan synthesis to bacterial growth and morphology. Nat Rev Micro 10, 123–136.

Ursell TS, Nguyen J, Monds RD, Colavin A, Billings G, Ouzounov N, Gitai Z, Shaevitz JW, and Huang KC (2014). Rod-like bacterial shape is maintained by feedback between cell curvature and cytoskeletal localization. Proc. Natl. Acad. Sci. USA.

van Teeffelen S, Wang S, Furchtgott L, Huang KC, Wingreen NS, Shaevitz JW, and Gitai Z (2011). The bacterial actin MreB rotates, and rotation depends on cell-wall assembly. Proc. Natl. Acad. Sci. USA 108, 15822–15827. [PubMed: 21903929]

Vasi F, Travisano M, and Lenski RE (1994). Long-term experimental evolution in Escherichia coli. II. Changes in life-history traits during adaptation to a seasonal environment. Am. Nat. 432–456.

Wang S, Arellano-Santoyo H, Combs PA, and Shaevitz JW (2010). Actin-like cytoskeleton filaments contribute to cell mechanics in bacteria. Proc. Natl. Acad. Sci. USA 107, 9182–9185. [PubMed: 20439764]

Wang S, Furchtgott L, Huang KC, and Shaevitz JW (2012). Helical insertion of peptidoglycan produces chiral ordering of the bacterial cell wall. Proc. Natl. Acad. Sci. USA 109, E595–E604. [PubMed: 22343529]

Wu C-Y, Rolfe PA, Gifford DK, and Fink GR (2010). Control of Transcription by Cell Size. PLoS Biology 8, e1000523. [PubMed: 21072241]

Author Manuscript Author Manuscript Author Manuscript Author Manuscript

Young KD (2006). The Selective Value of Bacterial Shape. Microbiol. Mol. Biol. Rev. 70, 660–703. [PubMed: 16959965]

Zhang W, Sehgal V, Dinh DM, Azevedo RBR, Cooper TF, and Azencott R (2012). Estimation of the rate and effect of new beneficial mutations in asexual populations. Theor Popul Biol 81, 168–178. [PubMed: 22155293]

Author Manuscript Author Manuscript Author Manuscript Author Manuscript

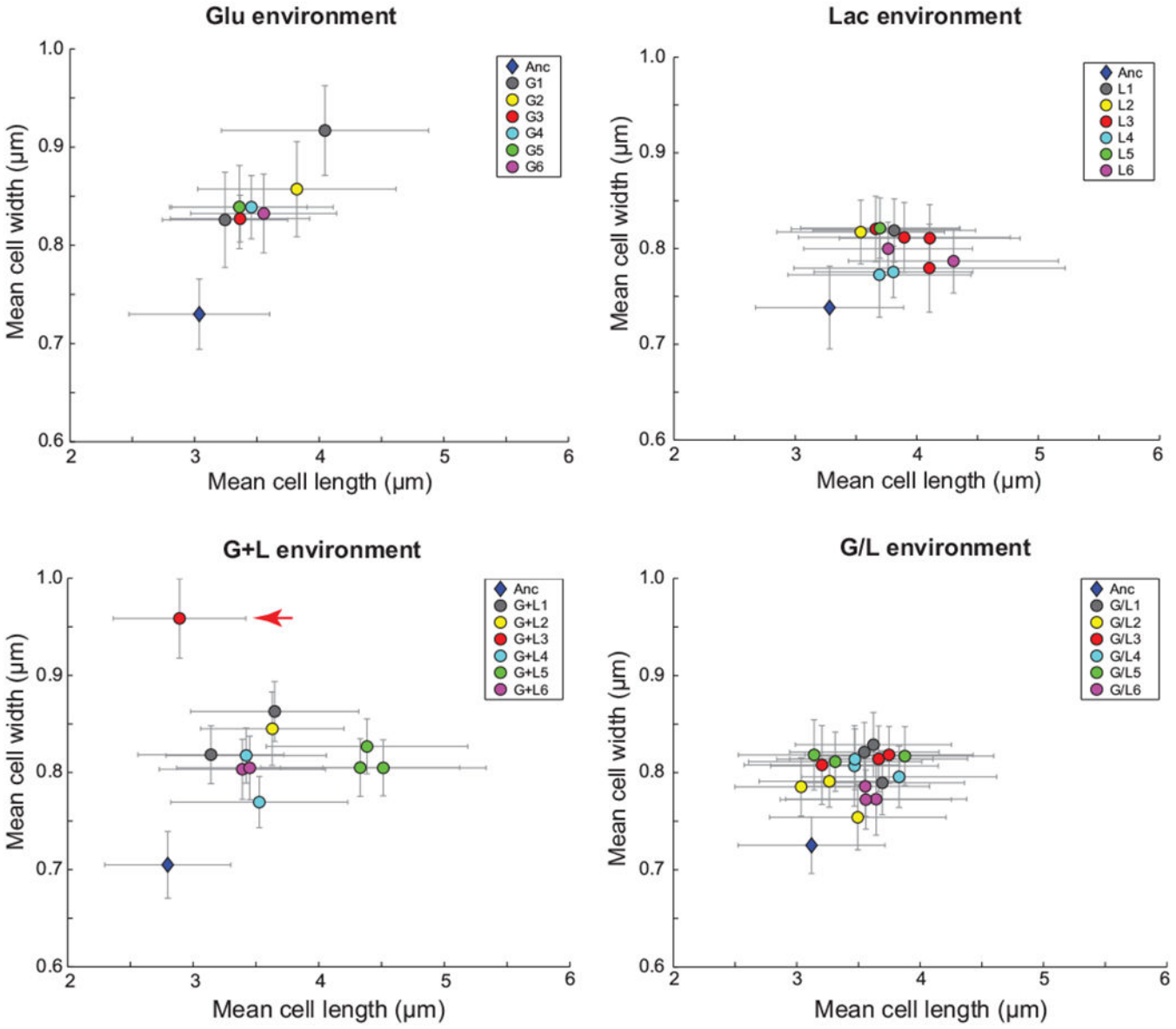


**Figure 1. Evolved clones exhibit increases in cell width and length.**

Clones from each of the 24 evolved populations were imaged during exponential growth in their respective evolution environments: Glu, Lac, G+L, or G/L. The nomenclature for evolved clones follows an E*x*-*y* format, where E is the environment (G, L, G+L, or G/L), *x* is the population and y is the clone isolated from this population. Clones are colored by population and some populations are represented by more than one independent clone (e.g. G1 has two clones, G1-1 and G1-2). An ancestral control is plotted for each environment (blue diamond). Clone G+L3 (clone isolated from the third evolved population in G+L) exhibited the largest width increase and is marked with a red arrow. Error bars represent standard deviations of the population distributions.

Author Manuscript Author Manuscript Author Manuscript Author Manuscript

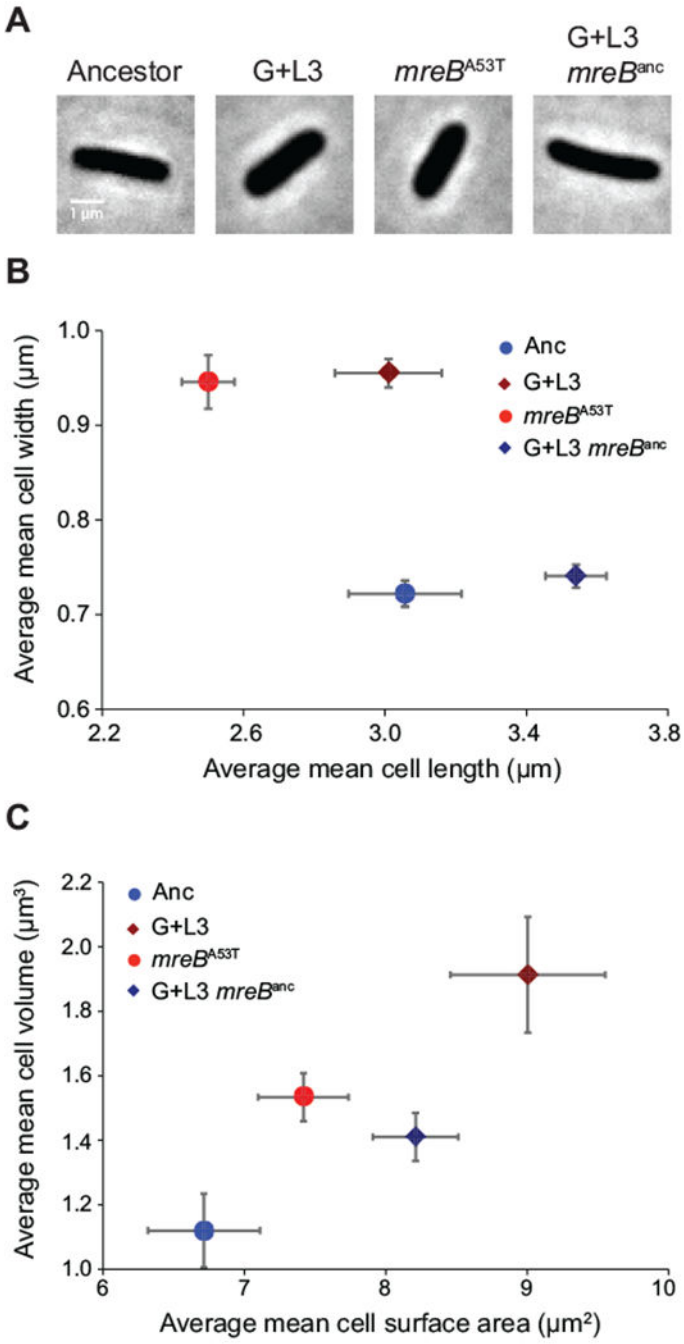


**Figure 2. The *mreB*$^{A53T}$ allele results in an increase in cell width and volume.**

A) Phase-contrast images of the ancestor (Anc), the evolved clone (G+L3), the ancestor carrying the *mreB*$^{A53T}$ allele (*mreB*$^{A53T}$), and the evolved clone with *mreB* reverted back to the ancestral sequence (G+L3 *mreB*$^{anc}$). B) Comparison of average mean cell width and length for each strain during exponential growth in Davis minimal medium plus glucose (DM+Glu). C) Comparison of average mean cell volume and surface area for each strain during exponential growth in DM+Glu. In (B,C), the ancestral and evolved strain backgrounds are represented by circles and diamonds, respectively. Blue symbols denote

Author Manuscript Author Manuscript Author Manuscript Author Manuscript

strains expressing the *mreB*$^{anc}$ allele and red symbols denote strains expressing the *mreB*$^{A53T}$ allele. All estimates of cell geometry are the average of three independent measures of population means derived from quantification of >200 cells. Error bars represent 95% confidence intervals (CIs).

Author Manuscript Author Manuscript Author Manuscript Author Manuscript

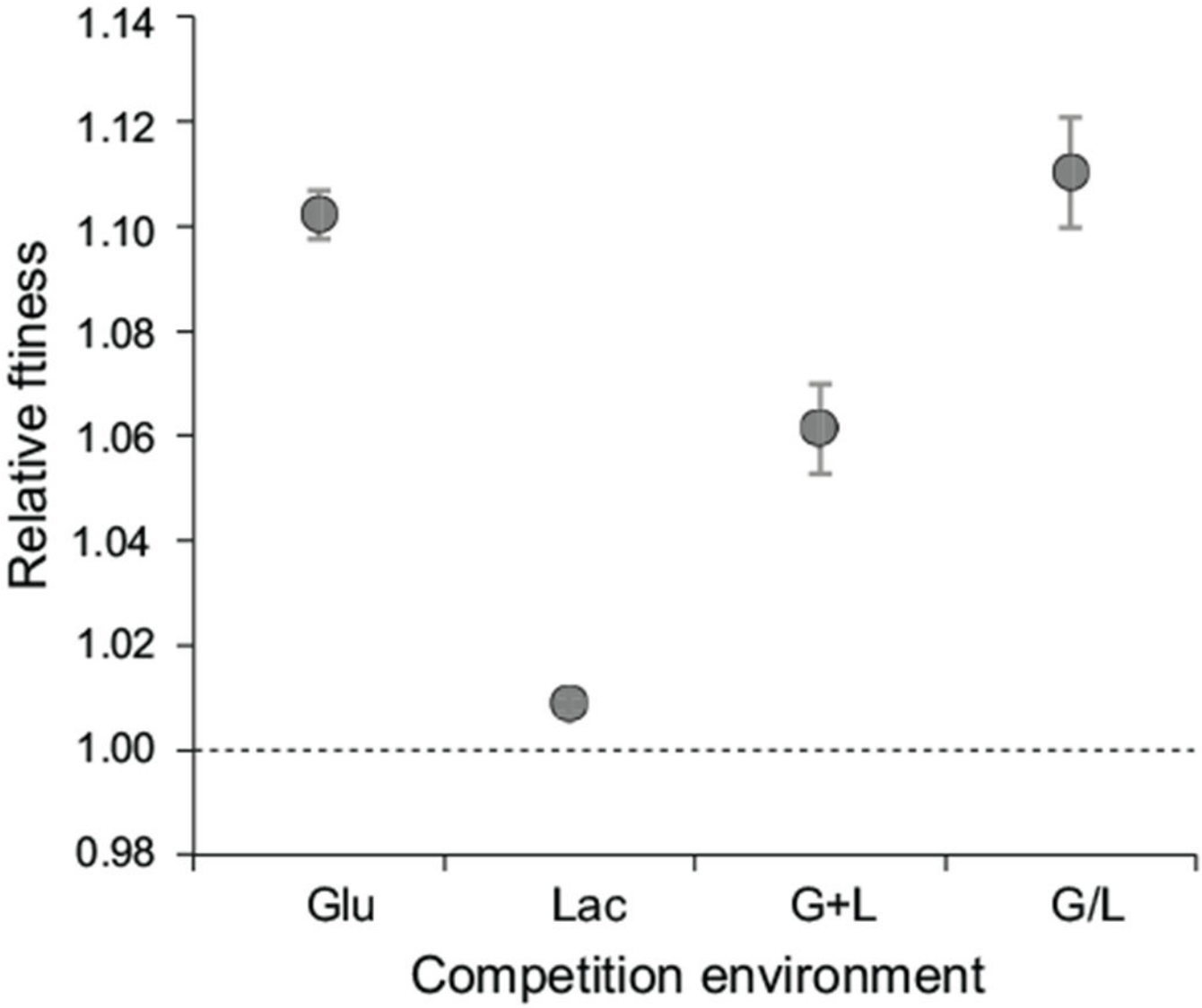


**Figure 3. The *mreB*$^{A53T}$ allele is adaptive.**

Head-to-head fitness competitions between the *mreB*$^{A53T}$ mutant and the ancestor were performed in four evolution environments: Glu, Lac, G+L, and G/L. Estimates for relative fitness are the average of eight replicates analyzed across two independent experiments. The dashed line represents zero difference in fitness. Error bars represent 95% CIs.

Author Manuscript Author Manuscript Author Manuscript Author Manuscript

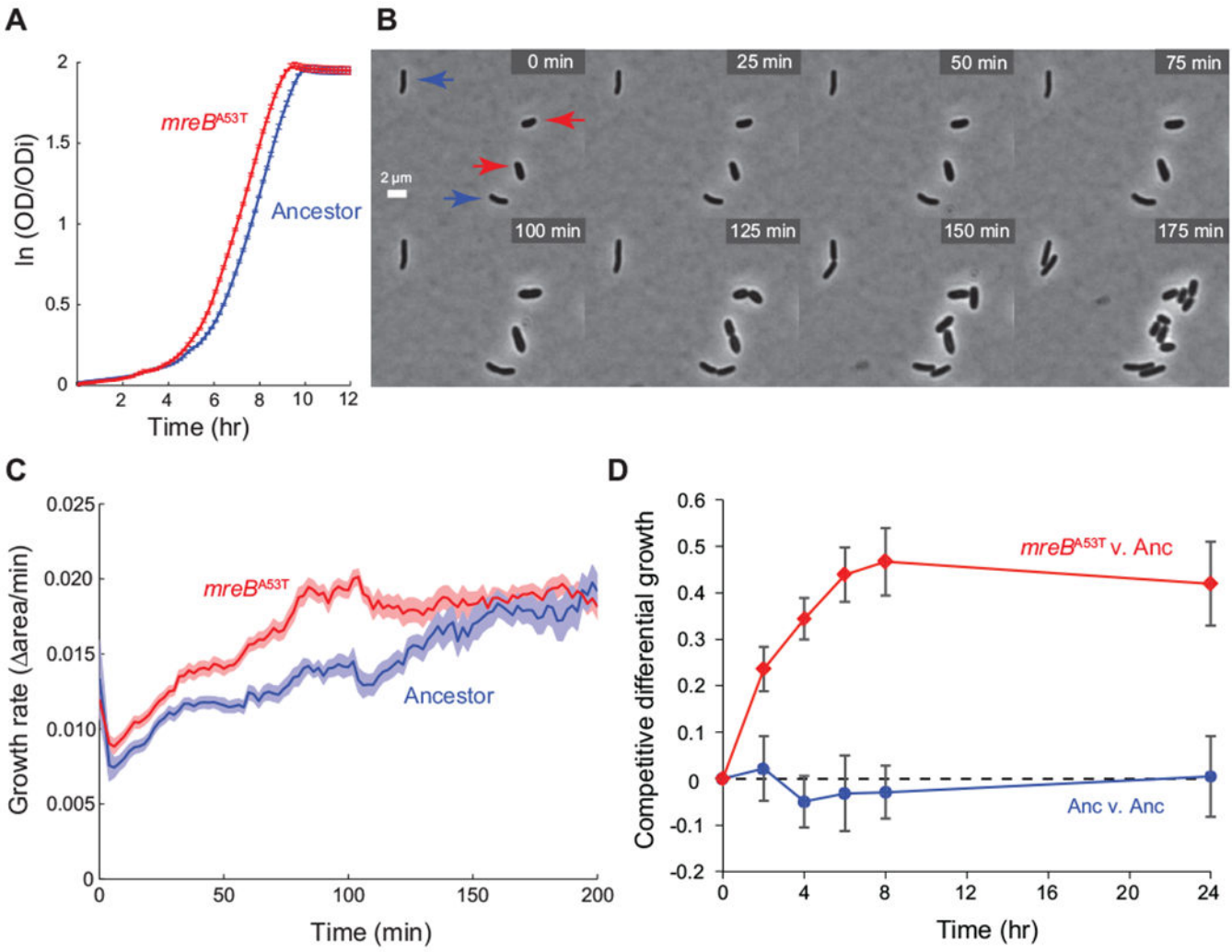


**Figure 4. The *mreB*$^{A53T}$ allele confers a lag-phase growth advantage.**

A) Population growth dynamics for the ancestor and the *mreB*$^{A53T}$ strain in Davis minimal medium plus glucose (DM+Glu). Optical density (OD) is normalized by the initial optical density ($OD_i$). Errors represent standard error ($n = 6$). B) Time-lapse images of the *mreB*$^{A53T}$ strain and the ancestor transitioning from stationary phase to exponential growth in DM+Glu medium. Ancestral and *mreB*$^{A53T}$ genotypes were distinguished based on differences in cell width, which have well separated distributions (Fig. 1 & Table S1). Red arrows indicate *mreB*$^{A53T}$ cells and blue arrows indicate ancestral cells. C) Instantaneous growth rates of single cells transitioning from stationary phase to exponential growth on DM +Glu indicate a decrease in lag phase time for *mreB*$^{A53T}$ cells. Growth rates were calculated as the fractional increase in the two-dimensional projected area of the cell between frames. Shaded boundaries represent standard error ($n = 20$). D) Fine-scale analysis of differential growth for the *mreB*$^{A53T}$ strain competed against the ancestor in the Glu environment. Competitive differential growth represents the natural log difference in growth between competitors relative to their initial density. As a control, the ancestor was also competed against itself and showed no growth differences over the course of competition. Error bars represent standard error ($n = 8$).

Author Manuscript Author Manuscript Author Manuscript Author Manuscript

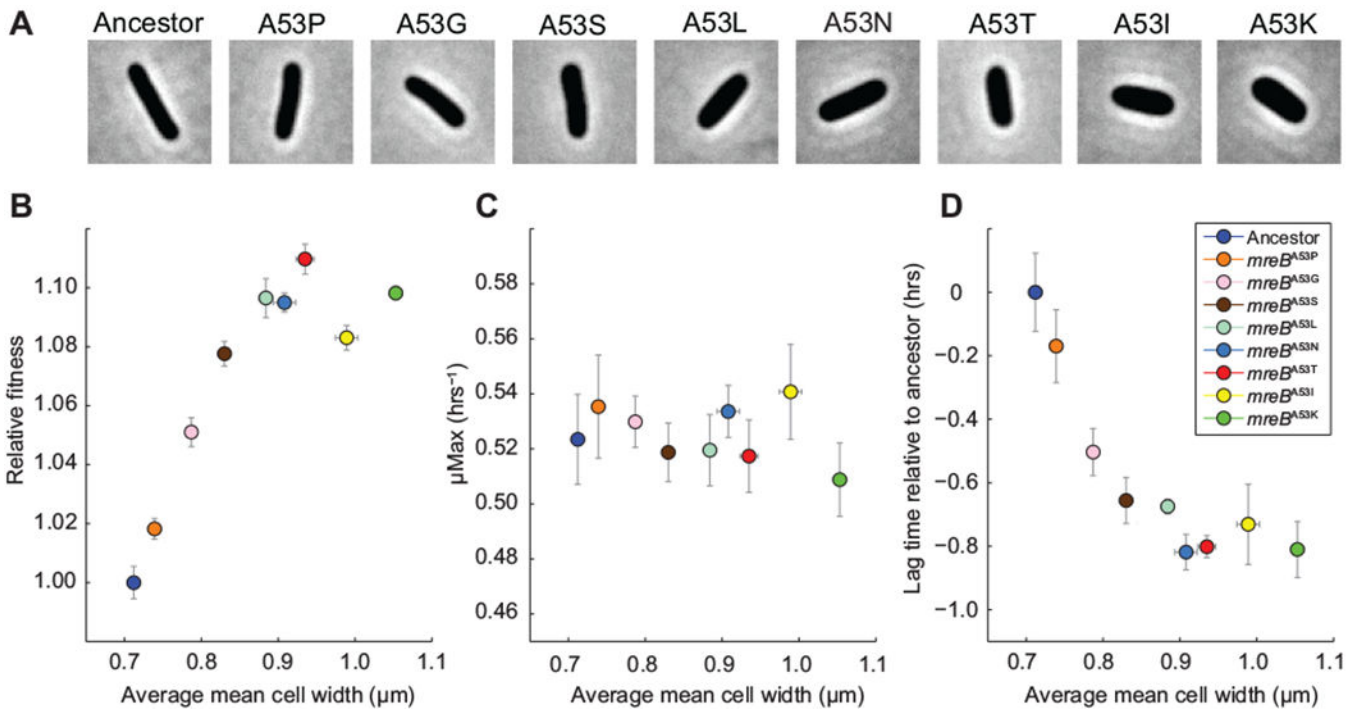


**Figure 5. Scaling between cell geometry and fitness.**

A) Phase-contrast images of *mreB*$^{A53}$ mutants. B) Head-to-head fitness competitions between *mreB*$^{A53}$ mutants and the ancestor were performed in the Glu environment. Estimates for relative fitness are the average of eight replicates across two independent experiments. Mean cell widths are the average of three independent estimates for each strain. Error bars for fitness and cell width measurements represent 95% CIs. C) Maximal growth rates of *mre*B$^{A53}$ mutants and the ancestor in DM+Glu as function of cell width. Error bars represent 95% CIs ($n$ = 8). D) Relative lag time of *mreB*$^{A53}$ mutants in DM+Glu as a function of cell width. Error bars represent 95% CIs ($n$ = 8).

Author Manuscript Author Manuscript Author Manuscript Author Manuscript

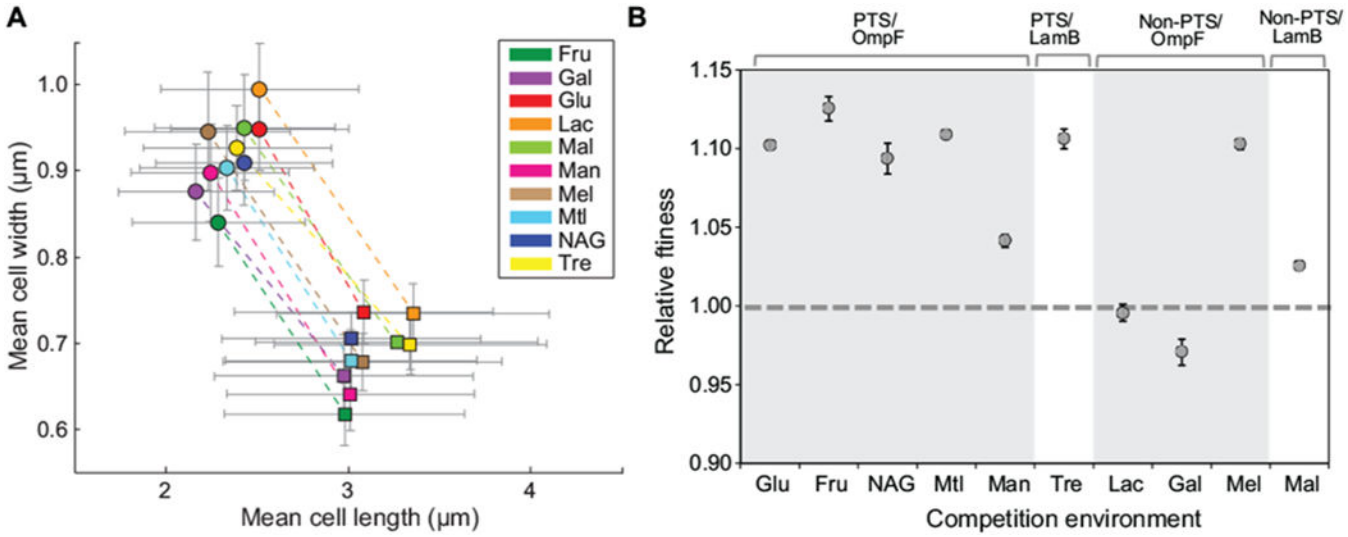


**Figure 6. Environment -dependent fitness effect**

A) Morphology of the ancestor and *mreB*$^{A53T}$ mutant in DM media supplemented with different carbon sources. Environments: Glu (glucose), Fru (fructose), NAG (N-acetyl glucosamine), Man (mannose), Lac (lactose), Gal (galactose), Mel (melibiose), Mal (maltose), and Tre (trehalose). Average mean values for cell width and length distributions are plotted. Dashed lines connect strains imaged in the same environment. Error bars represent standard deviations of the population distributions; the ancestor is represented by square symbols and the *mreB*$^{A53T}$ strain by circular symbols. B) Head-to-head competitions were performed between the ancestor and the *mreB*$^{A53T}$ mutant strain in the same environments shown in (A). Estimates for relative fitness are the average of eight replicates analyzed across two independent experiments. The dashed line represents zero difference in fitness. Error bars represent 95% CIs.